Supplementary Information (SI) for Soft Matter.

Supporting Information

Coconut Pollen Paper Soft Actuator: Tunable Shape Morphism Driven by Vapor

Sarah Ahmad Siraj,[†,‡] Vipin Kumar,[†,‡] Akash Patil,[¶,‡] Ratna K. Annabattula,[¶,‡] and Dillip K. Satapathy[*,†,‡]

†*Soft Materials Laboratory, Department of Physics, IIT Madras, Chennai-600036, Tamil Nadu, India*

‡*Center for Soft and Biological Matter, IIT Madras, Chennai-600036, Tamil Nadu, India*

¶*Stimuli Responsive Systems Lab, Department of Mechanical Engineering, IIT Madras, Chennai-600036, Tamil Nadu, India*

E-mail: dks@iitm.ac.in

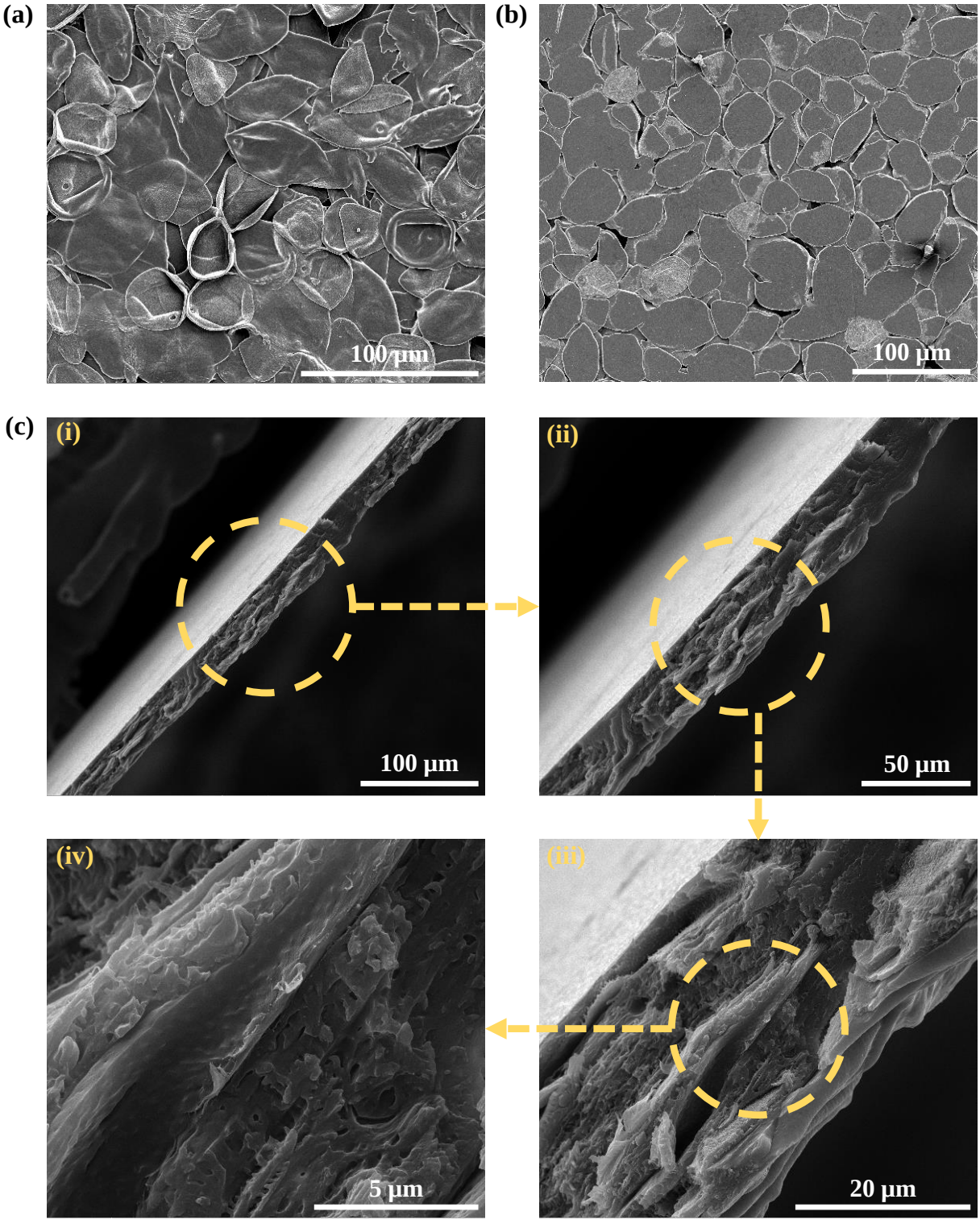

Supporting Fig. 1: FESEM image of the (a) top surface of pollen paper (T) and (b) bottom surface of pollen paper (B). (c) FESEM images of the cross-section of pollen paper magnified at different length scales with magnifications (i) 800×, (ii) 1500×, (iii) 6000× and (iv) 22008×.

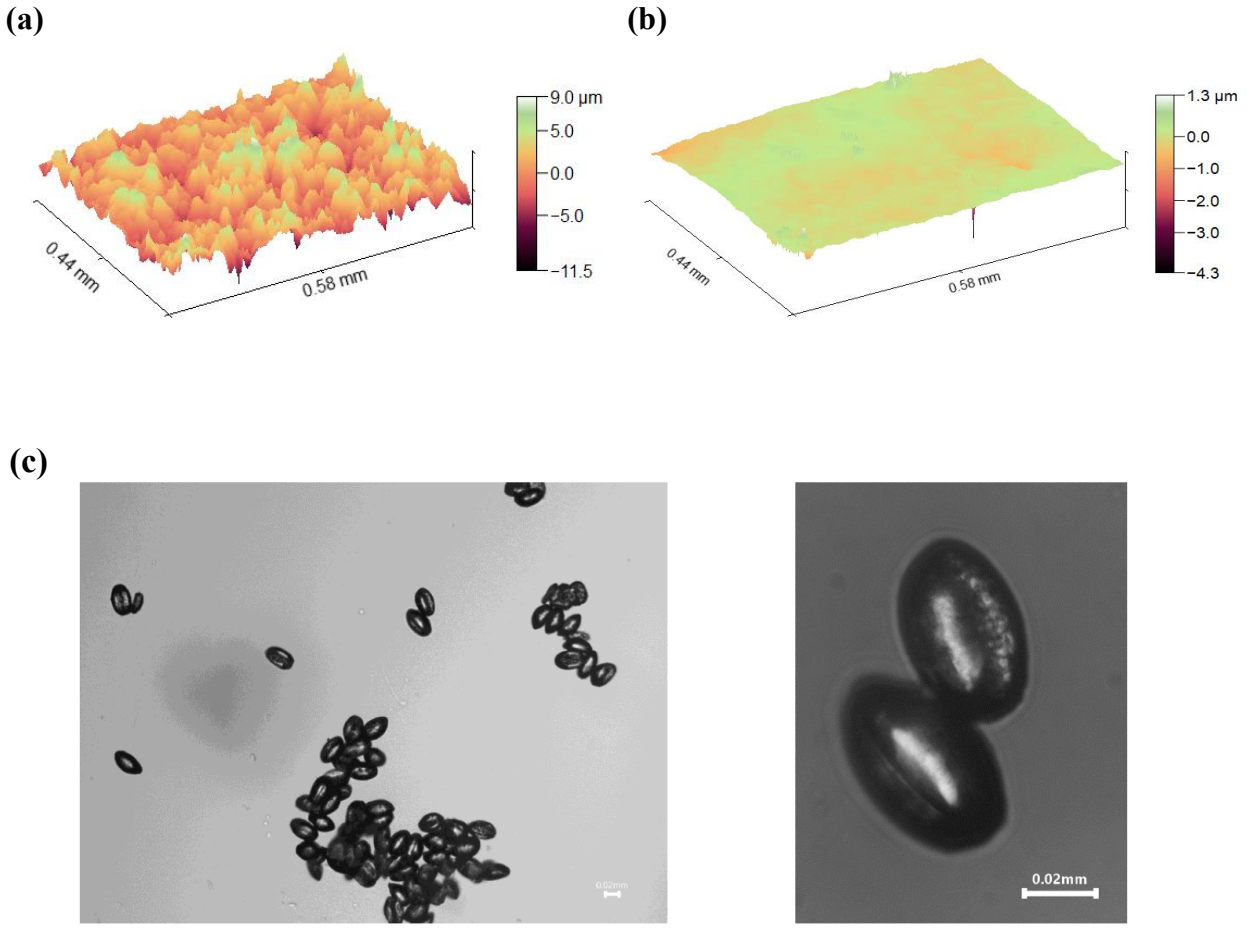

Supporting Fig. 2: 3D height profilometry images of (a) top surface (T) and (b) bottom surface (B) of the pollen paper. The dimensions of the scanned areas are marked. (c) Images of the coconut pollen grains recorded by optical microscope. The grains are approximately 60 µm in length and exhibit a single longitudinal furrow along their axis.

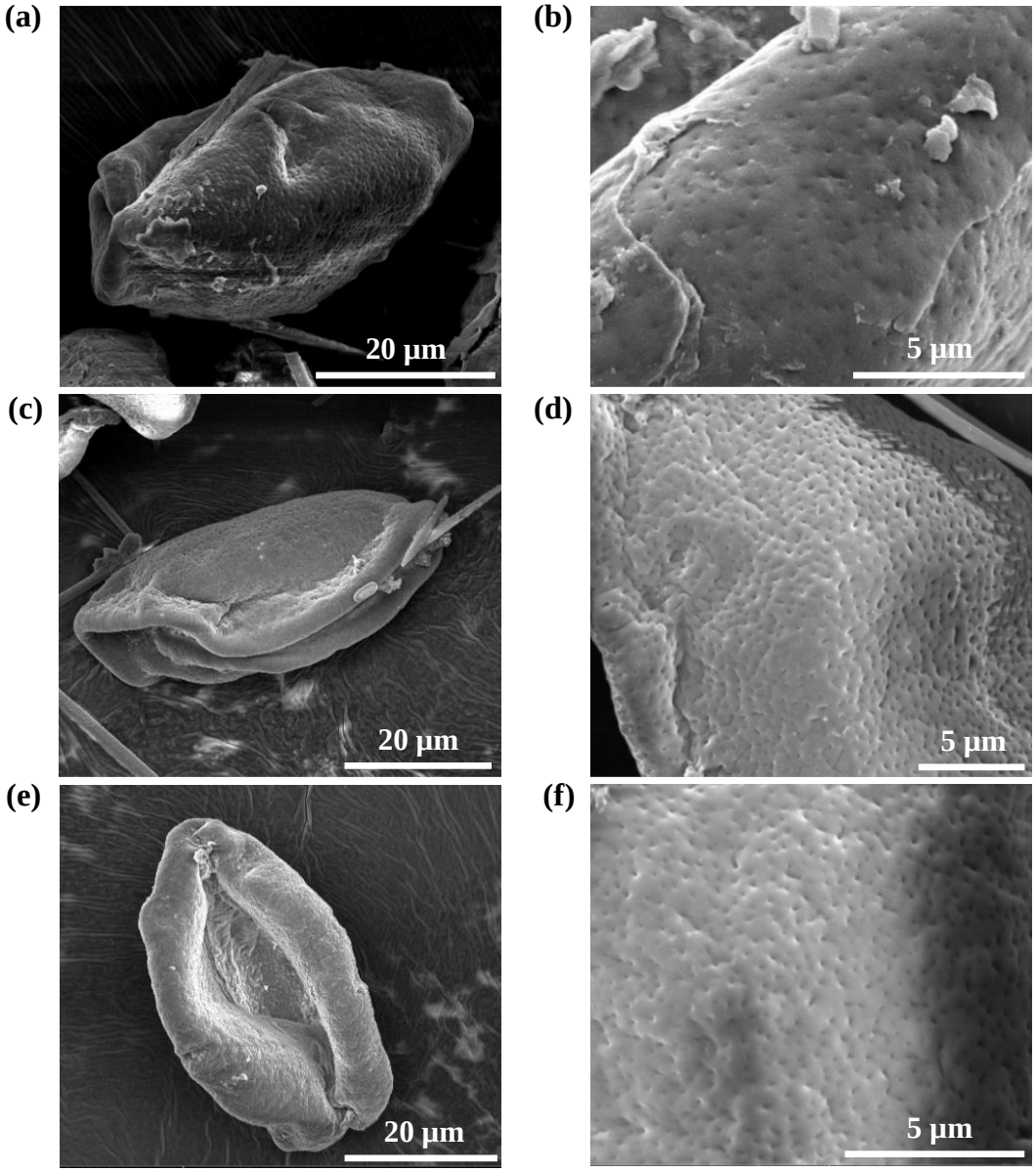

(g)

Element	WW	AD	OD
	Weight %		
C	90.0	91.7	96.5
N	3.0	2.3	0.1
O	7.0	6.0	3.4

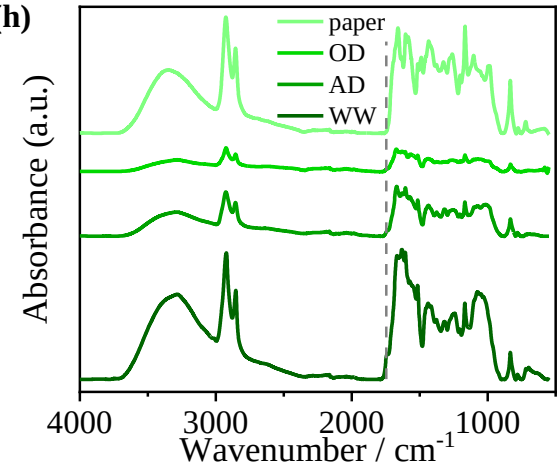

Supporting Fig. 3: FESEM images of (a) coconut bee pollen grain after WW; (b) surface of pollen grain after WW; (c) pollen grain after AD; (d) surface of pollen grain after AD; (e) pollen grain after OD; (f) surface of pollen grain after OD. (g) EDAX analysis of pollen grains after each step of preparation. (h) ATR-FTIR absorbance spectra of different steps in the preparation of the pollen paper and the final pollen paper.

Calculation of Young's modulus:

The indentation was carried out using a diamond Berkovich indenter having Young's modulus, $E_{\mathrm{i}} = 1140\,\mathrm{GPa}$ and Poisson's ratio, $\nu_i = 0.07$. From the obtained load-displacement curves, once the stiffness (S) and the contact area $A(h_c)$ as a function of contact depth (h_c) were obtained, the reduced Young's modulus (E_{r}) was obtained using the Oliver-Pharr equation:[1]

$$E_{\mathrm{r}} = \frac{\sqrt{\pi} S}{2\sqrt{A(h_c)}} \tag{1}$$

The pollen papers' Young's modulus ($E_{\mathrm{s}} = 1.139\,\mathrm{GPa}$) was then obtained from E_{r} using,[2]

$$\frac{1}{E_{\mathrm{r}}} = \frac{(1-\nu_s^2)}{E_{\mathrm{s}}} + \frac{(1-\nu_i^2)}{E_{\mathrm{i}}} \tag{2}$$

where ν_s is the sample Poisson ratio usually taken 0.5 for biological samples.[3]

To verify the consistency of samples prepared across different batches, we measured the Young's modulus of pollen papers fabricated from three independent batches. The mean Young's modulus was found to be $(1.68 \pm 0.56)\,\mathrm{GPa}$, indicating good reproducibility across batches. These values lie within a relatively narrow range,[4] further confirming the reliability of our fabrication process.

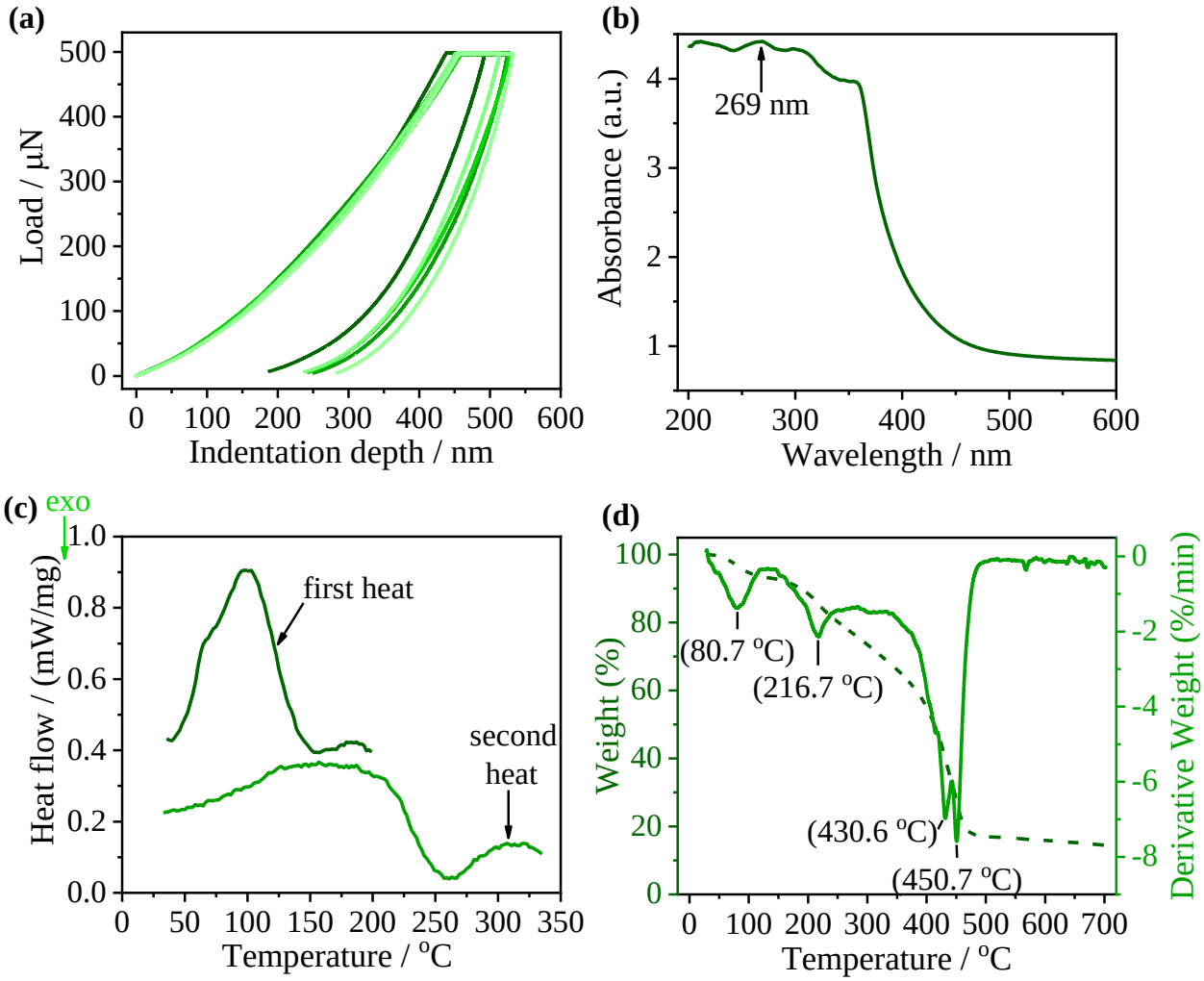

Supporting Fig. 4: (a) Nano-indentation load-displacement curves of 5 different locations on the pollen paper. (b) UV-Vis absorption spectra of pollen paper. (c) DSC data of pollen paper with exothermic down. (d) TG-DTA curve of pollen paper.

Effect of heat and UV treatment:

Pollen papers were heated for 30 minutes at 50 °C in one experiment and exposed to UV light at a wavelength of 254 nm for 3 minutes in a UV chamber for another experiment. The actuation response of the pollen paper on exposure to water vapor was recorded before and after the treatments. The experiment was repeated multiple times with pollen papers of different aspect ratios and one curvature vs. time plot is shown in Supporting Fig. 5(a) and (b). All of our experiments resulted in a slight increase in the curvature of the pollen paper after the treatments.

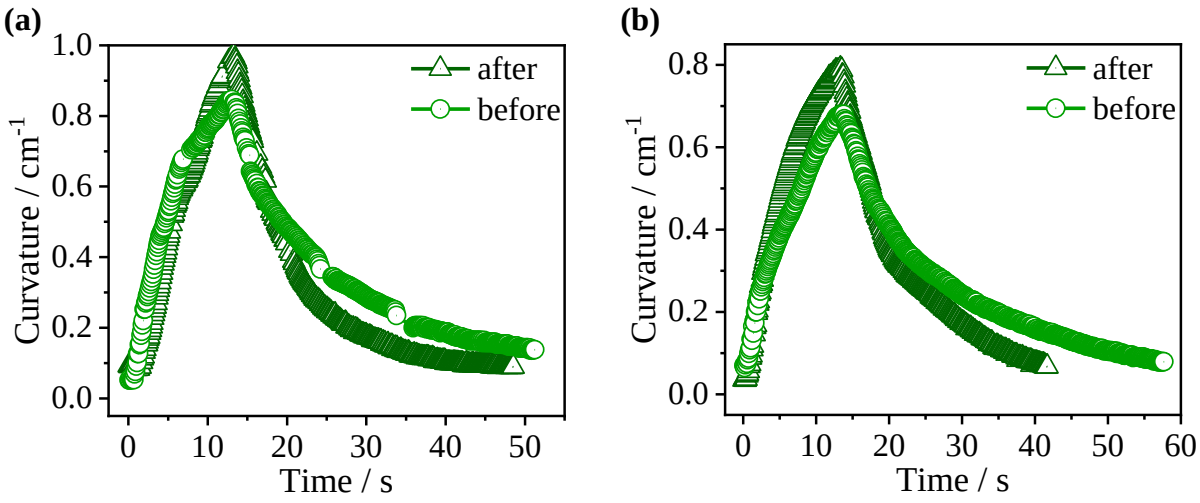

Supporting Fig. 5: (a) The actuation response of pollen paper when exposed to water vapor before and after heating for 30 minutes at 50 °C. The dimensions of the pollen paper are (2.30 ± 0.05) cm$\times(1.50 \pm 0.05)$ cm$\times(43 \pm 1)$ µm. (b) The actuation response of pollen paper when exposed to water vapor before and after exposure to 254 nm UV radiation for 3 minutes.

Effect of geometry on actuation:

The actuation behavior of the pollen paper upon exposure to water vapor was studied by controlling a) thickness and b) aspect ratio.

a) **Effect of thickness:** Pollen papers of different thicknesses ((17 ± 1) µm, (26 ± 1) µm, and (38 ± 1) µm were prepared by varying the volume of pollen solution in the petri dish. The pollen papers in a cantilever-like geometry were exposed to water vapor for 3 seconds from the bottom side. The (17 ± 1) µm thick pollen paper attained a maximum curvature of $2.564\,\mathrm{cm}^{-1}$. As the thickness was increased to (26 ± 1) µm and (38 ± 1) µm, the maximum curvature decreased to $2.030\,\mathrm{cm}^{-1}$ and $0.864\,\mathrm{cm}^{-1}$, respectively. The snapshots during the actuation of the above mentioned thicknesses are shown in Supporting Fig. 6(a), and the corresponding evolution of curvatures is plotted in Supporting Fig. 6(b).

   It is noted that the bending stiffness (k_b) of pollen paper increased with the increase in thickness and is calculated using the formula,

$$k_\mathrm{b} = E_\mathrm{s} \times I \tag{3}$$

   where E_s is the Youngs' modulus of the pollen paper and $I \propto \mathrm{thickness}^3$ is the moment of inertia. The bending stiffness of the (17 ± 1) µm, (26 ± 1) µm and (38 ± 1) µm thick pollen paper is thus calculated to be $4.6633 \times 10^{-9}\,\mathrm{Nm}^2$, $1.6683 \times 10^{-8}\,\mathrm{Nm}^2$ and $5.2083 \times 10^{-8}\,\mathrm{Nm}^2$, respectively. The increased bending stiffness with the increase in the thickness of pollen paper, greatly resists the moment generated by the absorption of water vapor in the pollen matrix.

b) **Effect of aspect ratio:** Four (26 ± 1) µm thick pollen papers of different aspect ratios were prepared by cutting into strips of dimensions $(1.00 \pm 0.05)\,\mathrm{cm} \times (1.00 \pm 0.05)\,\mathrm{cm}$ $(\mathrm{l}_1\mathrm{w}_1)$, $(1.00 \pm 0.05)\,\mathrm{cm} \times (1.20 \pm 0.05)\,\mathrm{cm}$ $(\mathrm{l}_1\mathrm{w}_2)$, $(1.30 \pm 0.05)\,\mathrm{cm} \times (1.00 \pm 0.05)\,\mathrm{cm}$

(l_2w_1) and $(1.30 \pm 0.05)\,\mathrm{cm} \times (1.20 \pm 0.05)\,\mathrm{cm}$ (l_2w_2). The cut strips of pollen paper were exposed to water vapor for 2 seconds from the bottom side. The curvatures obtained for l_1w_1, l_1w_2, l_2w_1 and l_2w_2 were $1.942\,\mathrm{cm}^{-1}$, $2.084\,\mathrm{cm}^{-1}$, $1.659\,\mathrm{cm}^{-1}$ and $1.829\,\mathrm{cm}^{-1}$ respectively, as shown in Supporting Fig. 6(c). First, for a constant length of l_1, an increase in the width from w_1 to w_2 led to larger curvature. As a larger width blocks the diffusion of water molecules over a larger area, a larger ΔRH across the pollen paper is created.[5] Similar results were obtained for pollen papers with constant lengths of l_2 and widths changing from w_1 to w_2. Second, for constant width w_1, an increase in the length from l_1 to l_2 led to a decrease in the overall curvature. We hypothesize that for the exposed area of the pollen paper, the generated dynamic local bending stresses are not enough to equally lift the pollen paper with a longer length. Similar results are obtained for pollen papers with constant width of w_2 and lengths changing from l_1 to l_2.

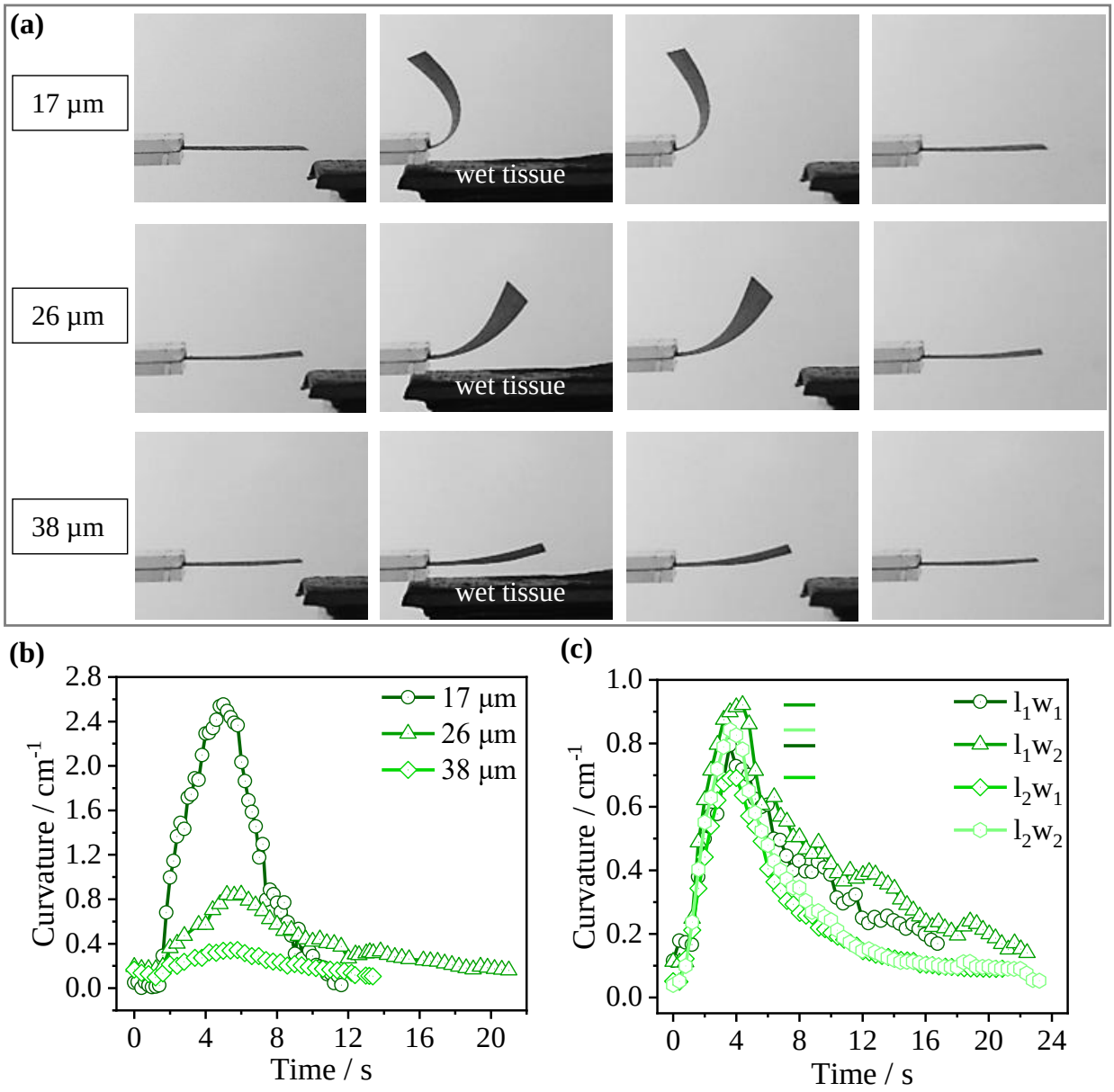

Supporting Fig. 6: (a) Snapshots of the response of pollen paper strips to water vapor originating from a wet tissue, with three different thicknesses $(17 \pm 1)\,\mu m$, $(26 \pm 1)\,\mu m$ and $(38 \pm 1)\,\mu m$. The length and width of all three pollen paper strips were maintained at $(1.00 \pm 0.05)\,cm \times (1.00 \pm 0.05)\,cm$, respectively. (b) The time evolution of curvature of pollen paper with three different thicknesses on exposure to water vapor. (c) The time evolution of curvature of pollen paper with $(29 \pm 1)\,\mu m$ thickness and varying aspect ratio when exposed to water vapor for 2 seconds from the bottom side. Here, the dimensions are l_1w_1: $(1.00 \pm 0.05)\,cm \times (1.00 \pm 0.05)\,cm$; l_1w_2: $(1.00 \pm 0.05)\,cm \times (1.20 \pm 0.05)\,cm$; l_2w_1: $(1.30 \pm 0.05)\,cm \times (1.00 \pm 0.05)\,cm$; l_2w_2: $(1.30 \pm 0.05)\,cm \times (1.20 \pm 0.05)\,cm$.

Estimation of vapor sorption required for actuation:

We consider the actuated state as the moment when the entire pollen paper becomes exposed to water vapor, shown in Supporting Fig. 7. The change in length of the pollen paper from the initial state (L) to the bent state (L') is

$$\Delta L = L' - L, \tag{4}$$

where L' = radius of curvature $\times$ central angle. Since actuation is driven by strain gradient across the paper thickness, we ignore the effect of change in thickness (t) and width (w) to estimate the amount of water sorption required for bending. Thus, the change in volume of the pollen paper can be estimated as:

$$\Delta V = w * t * \Delta L \tag{5}$$

Considering the volume occupied by one water molecule (V_{H_20}) as $3 \times 10^{-29}\,\mathrm{m}^3$,[6] the number of absorbed water molecules in the papers actuated state is obtained from:

$$\frac{\Delta V}{V_{H_20}} \tag{6}$$

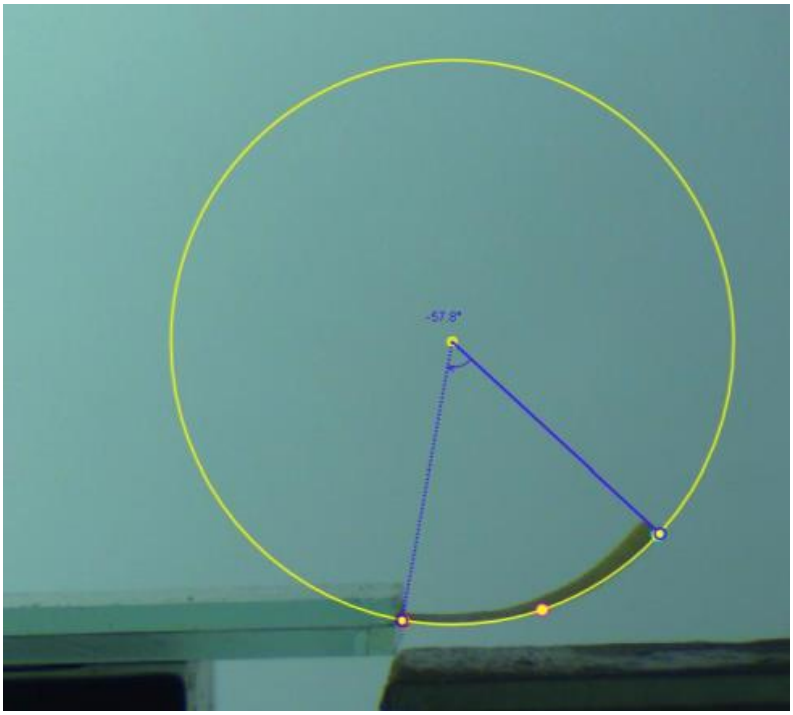

Supporting Fig. 7: The snapshot of the bending of pollen paper upon complete exposure to water vapor. The radius of curvature is 1.226 cm and the central angle is 57.8 rad.

Calculation of diffusion coefficient using DVS:

To understand the sorption kinetics of water into the pollen paper, a 'parallel exponential kinetics' (PEK) model has been used on the DVS data. The PEK equation[7] is given as:

$$MC = MC_0 + MC_1(1 - e^{\frac{-t}{t_1}}) + MC_2(1 - e^{\frac{-t}{t_2}}) \tag{7}$$

where MC and MC_0 are the moisture contents at infinite time of water vapor exposure at a constant RH and at time zero, respectively. The two exponential terms represent a fast and a slow process, having characteristic time of t_1 and t_2 and moisture content MC_1 and MC_2, respectively.

The temporal evolution of the MC, along with the best fit of the PEK model is plotted in Supporting Fig. 8(b)). The fitting parameters obtained from the best fit to the measured MC data are given in Supporting Table. 1.

The diffusion coefficient D, of water vapor through the pollen paper is estimated using:[8]

$$\frac{M_\mathrm{t}}{M_\infty} = \frac{4}{d}\sqrt{\frac{Dt}{\pi}}, \tag{8}$$

where, M_t is the mass of sorbed molecules at time t, M_∞ is the mass of sorbed molecules at equilibrium and d is the thickness of the pollen paper undergoing DVS.

Supporting Table 1: The best fit parameters of the PEK model and their values fitted over the DVS data.

Parameter	**Fit value**
MC_0	$(2.80 \pm 0.17)\%$
MC_1	$(28.00 \pm 0.51)\%$
MC_2	$(7.15 \pm 0.53)\%$
t_1	$(8.22 \pm 0.19)min$
t_2	$(34.70 \pm 1.85)min$

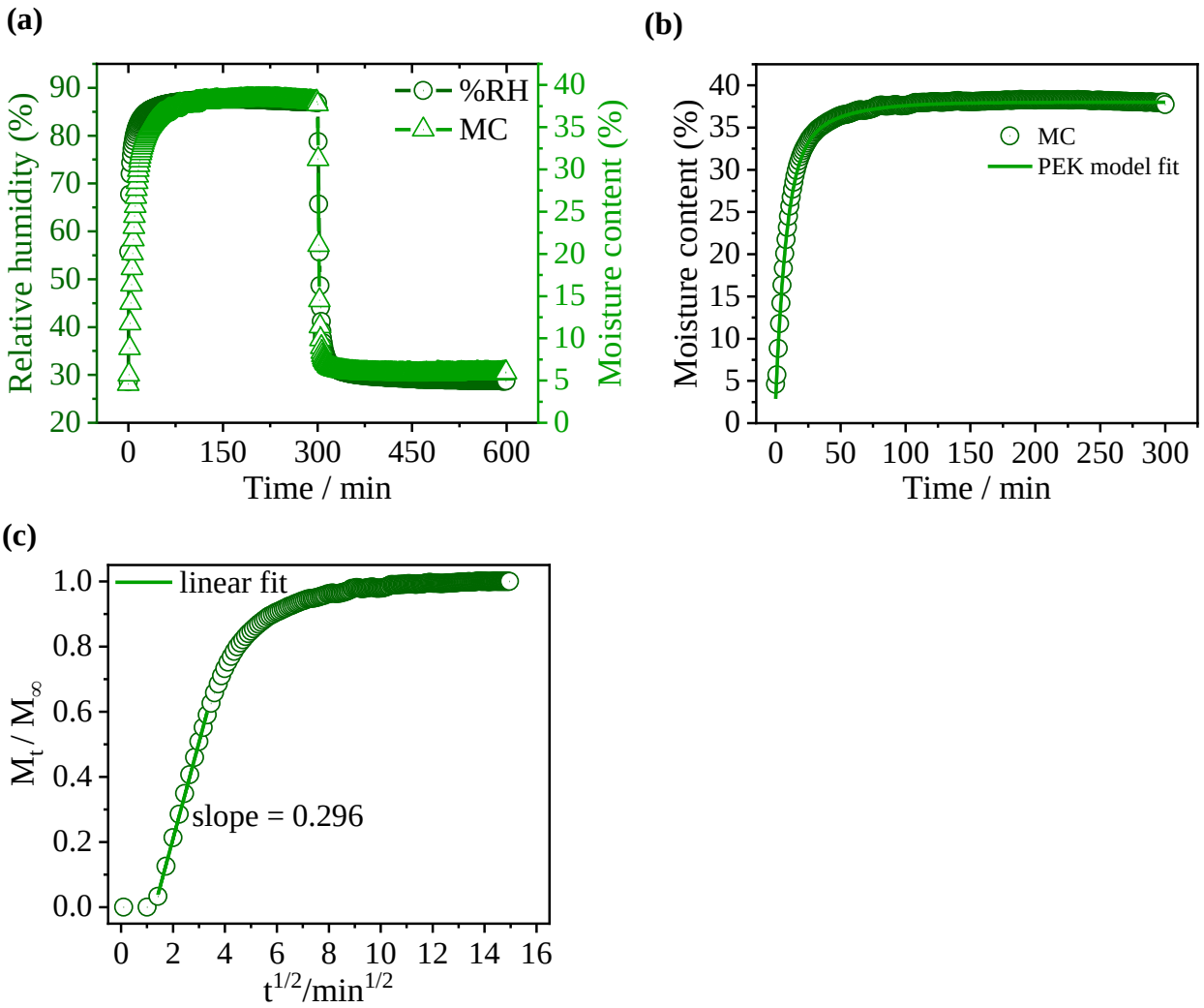

Supporting Fig. 8: (a) The plot shows the evolution of moisture content in the pollen paper as the humidity within the DVS chamber ramps up from 30 % RH to 90 % RH. It is observed that as the humidity remains constant for approximately 5 hours, the moisture content of the pollen paper also remains unchanged. With a sudden decrease in humidity to 30 % RH, the moisture content in the pollen paper also decreases. (b) The temporal evolution of moisture content of the pollen paper and the corresponding fit using the PEK model described in Supporting Eq. 7. (c) Calculation of the short-time diffusion coefficient using Supporting Eq. 8.

Effect of corrugation parameters on actuation:

The effect of the orientation of the corrugation was studied by changing its alignment with respect to the long axis of the pollen papers. This resulted in the pollen papers always actuating along the direction of the corrugations.

To investigate the influence of corrugation frequency and amplitude on the actuation behavior of pollen paper, FEA simulations were performed on square-shaped corrugated specimens. As a reference configuration, a square pollen paper with a corrugation depth of 30 µm and ten corrugations was considered. Using the parameters specified in the Experimental Section, the corrugation depth was systematically varied from 10 µm to 50 µm, while keeping the number of corrugations constant. The resulting curvatures were computed and are presented in Supporting Fig. 9(a).

Subsequently, the number of corrugations was varied from zero (uncorrugated pollen paper) to three times the reference frequency, while maintaining a constant depth of 30 µm. The corresponding curvatures are plotted in Supporting Fig. 9(b).

In both cases, the overall change in actuation curvature remained modest due to the relatively small size of the corrugations compared to the overall thickness of the specimen. Nevertheless, a clear trend of increasing curvature with increasing corrugation depth and frequency was observed.

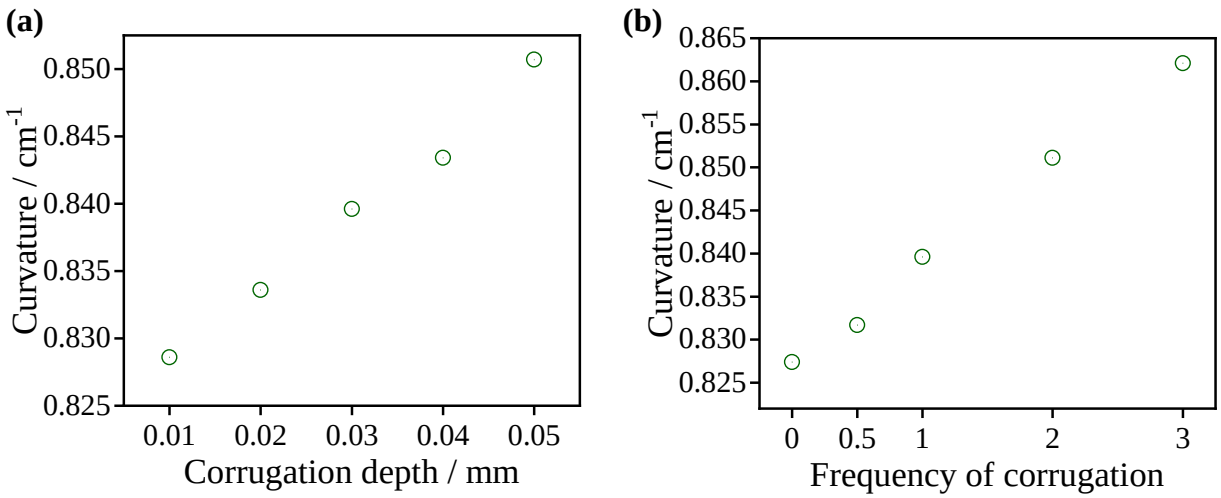

Supporting Fig. 9: Evolution of curvature as a function of (a) corrugation depth and (b) corrugation frequency, obtained from FEA simulations on a square-shaped corrugated pollen paper.

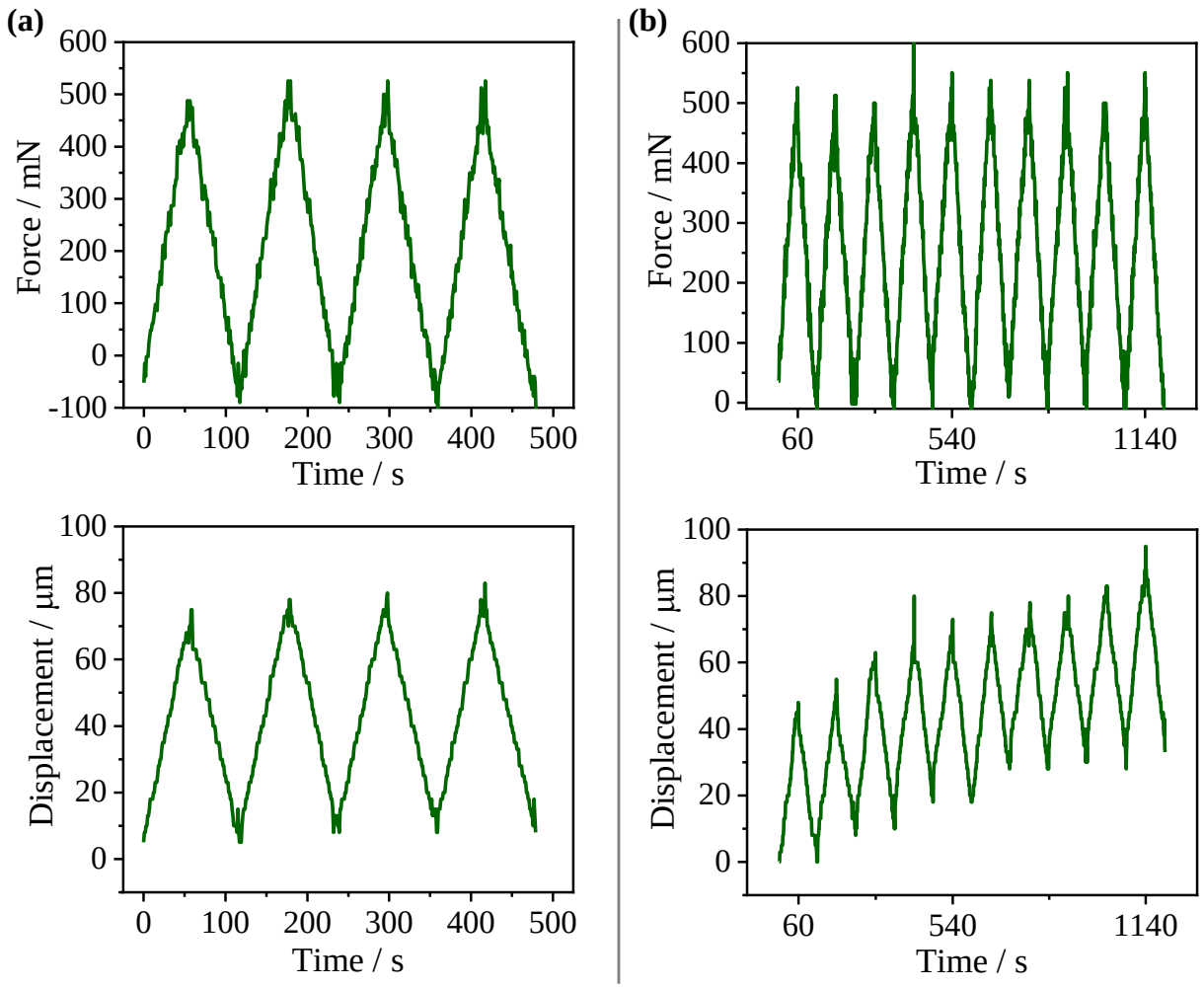

Supporting Fig. 10: (a) Force–time plot for tensile testing of pollen paper under ambient humidity, with the corresponding displacement–time evolution. (b) Force–time plot for tensile testing of pollen paper during one-sided exposure to water vapor, along with the corresponding displacement–time evolution.

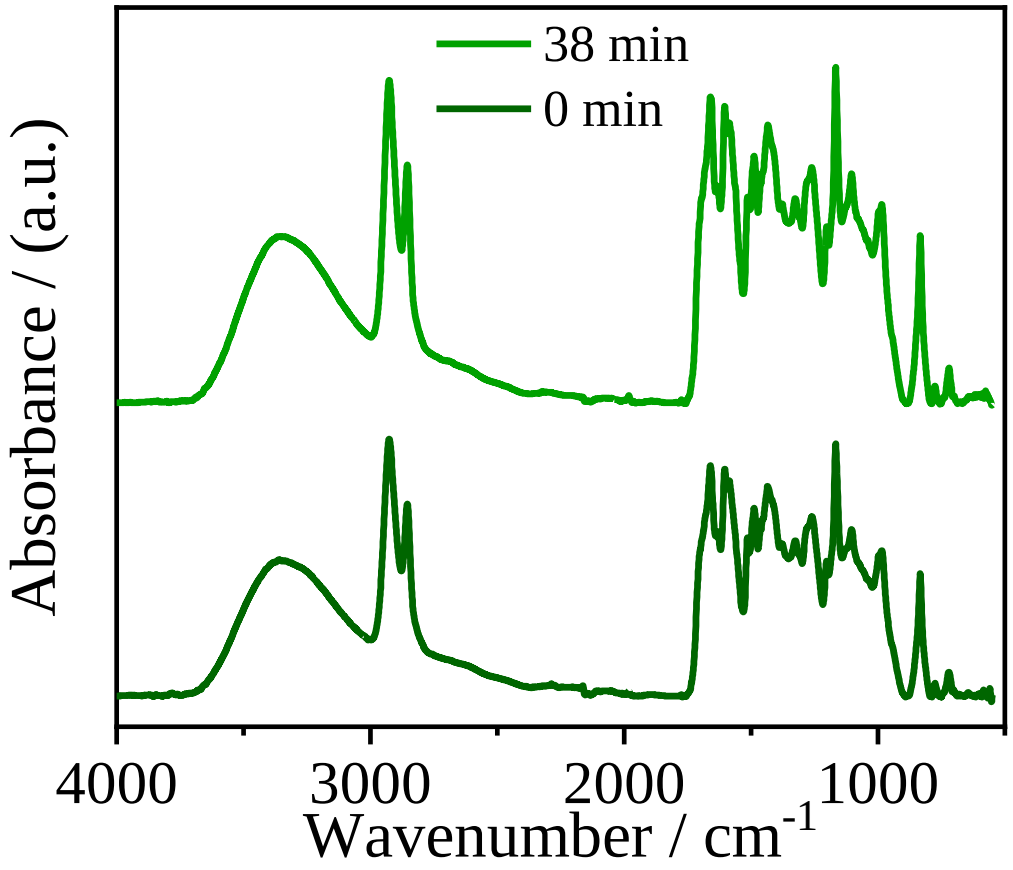

Supporting Fig. 11: ATR-FTIR spectra of pollen paper before (0 min) and after 38 minutes of exposure to water vapor. No noticeable change in the characteristic functional group peaks are observed, confirming the absence of chemical alterations in the pollen structure.

Supporting Table 2: Comparative summary of material characteristics, actuation response, and bending-axis controllability for a range of polymer-based vapor-responsive soft actuators.

Polymer	Thickness	Vapor Type	Response Time	Maximum Actuation	Bending Axis Control	Reference
PDMS	1500 µm	Ethanol	–	360°	No	[9]
Nafion	75 µm	Ethanol	0.25 s	0.31 mm^{-1}	Yes	[10]
CNF/GO/CNT	8 µm	Water	2 s	90°	No	[11]
CNF/MXene/Tannic acid	15 µm	Water	3 s	156°	No	[12]
RGO-CF/GO-CF	–	Water	6 s	1.48 cm^{-1}	No	[13]
CNF	7 µm	Water	3 s	0.15 cm^{-1}	No	[14]
Tapioca starch	(18 ± 1) µm	Water	1.84 s	1.65 cm^{-1}	Yes	[15]
Bombyx mori silk	8 µm	Water	3 s	1.65 cm^{-1}	Yes	[16]
Sunflower pollen	27 µm	Water	80 s	1.6 cm^{-1}	No	[3]
Coconut pollen	(17 ± 1) µm	Water	3 s	2.56 cm^{-1}	**Yes**	**This work**

Supporting References

(1) Wang, Y.; Porter, D. L.; Naleway, S. E.; Newell, P. Thermo-mechanical characterization of shale using nanoindentation. *Scientific Reports* **2021**, *11*, 1–12.

(2) Young, T. J.; Monclus, M. A.; Burnett, T. L.; Broughton, W. R.; Ogin, S. L.; Smith, P. A. The use of the PeakForceTM quantitative nanomechanical mapping AFM-based method for high-resolution Young's modulus measurement of polymers. *Measurement Science and Technology* **2011**, *22*, 125703.

(3) Zhao, Z.; Hwang, Y.; Yang, Y.; Fan, T.; Song, J.; Suresh, S.; Cho, N. J. Actuation and locomotion driven by moisture in paper made with natural pollen. *Proceedings of the National Academy of Sciences of the United States of America* **2020**, *117*, 8711–8718.

(4) Qu, Z.; Meredith, J. C. The atypically high modulus of pollen exine. *Journal of the Royal Society Interface* **2018**, *15*, 20180533.

(5) Treml, B. E.; McKenzie, R. N.; Buskohl, P.; Wang, D.; Kuhn, M.; Tan, L. S.; Vaia, R. A. Autonomous Motility of Polymer Films. *Advanced Materials* **2018**, *30*, 1–6.

(6) Likić, V. A.; Prendergast, F. G.; Juranić, N.; Macura, S. A "structural" water molecule in the family of fatty acid binding proteins. *Protein Science* **2000**, *9*, 497–504.

(7) Hill, C. A.; Norton, A. J.; Newman, G. The water vapour sorption properties of Sitka spruce determined using a dynamic vapour sorption apparatus. *Wood Science and Technology* **2010**, *44*, 497–514.

(8) Chin, J. W.; Nguyen, T.; Aouadi, K. Sorption and Diffusion of Water, Salt Water, and Concrete Pore Solution in Composite Matrices. *Journal of Applied Polymer Science* **1999**, *71*, 483–492.

(9) Zheng, L.; Dong, S.; Nie, J.; Li, S.; Ren, Z.; Ma, X.; Chen, X.; Li, H.; Wang, Z. L. Dual-stimulus smart actuator and robot hand based on a vapor-responsive PDMS film

and triboelectric nanogenerator. *ACS Applied Materials & Interfaces* **2019**, *11*, 42504–42511.

(10) Mu, J.; Wang, G.; Yan, H.; Li, H.; Wang, X.; Gao, E.; Hou, C.; Pham, A. T. C.; Wu, L.; Zhang, Q., et al. Molecular-channel driven actuator with considerations for multiple configurations and color switching. *Nature communications* **2018**, *9*, 590.

(11) Wei, J.; Jia, S.; Guan, J.; Ma, C.; Shao, Z. Robust and highly sensitive cellulose nanofiber-based humidity actuators. *ACS applied materials & interfaces* **2021**, *13*, 54417–54427.

(12) Wei, J.; Jia, S.; Wei, J.; Ma, C.; Shao, Z. Tough and multifunctional composite film actuators based on cellulose nanofibers toward smart wearables. *ACS applied materials & interfaces* **2021**, *13*, 38700–38711.

(13) Mao, J.-W.; Chen, Z.-D.; Han, D.-D.; Ma, J.-N.; Zhang, Y.-L.; Sun, H.-B. Nacre-inspired moisture-responsive graphene actuators with robustness and self-healing properties. *Nanoscale* **2019**, *11*, 20614–20619.

(14) Li, B.; Zhu, X.; Xu, C.; Yu, J.; Fan, Y. A tough, reversible and highly sensitive humidity actuator based on cellulose nanofiber films by intercalation modulated plasticization. *Carbohydrate Polymers* **2024**, *335*, 122108.

(15) Kumar, V.; Siraj, S. A.; Satapathy, D. K. Multivapor-Responsive Controlled Actuation of Starch-Based Soft Actuators. *ACS Applied Materials and Interfaces* **2024**, *16*, 3966–3977.

(16) Siraj, S. A.; Kumar, V.; Satapathy, D. K. Polymorphic Phase-Dependent Vapor-Responsive Actuation in Silk Fibroin Films: Control of Bending Angle and Axis. *Langmuir* **2025**,